International Journal of Fluid Machinery and Systems
Vol. 3, No. 3, July-September 2010

DOI: 10.5293/IJFMS.2010.3.3.235
ISSN (Online): 1882-9554

Review Paper

Moment Whirl due to Leakage Flow in the Back Shroud Clearance of a Rotor

Yoshinobu Tsujimoto[1], Zhenyue Ma[2], Bingwei Song[2], and Hironori Horiguchi[1]

[1] Graduate School of Engineering Science, Osaka University
1-3 Machikaneyama, Toyonaka, Osaka, 560-8531, Japan
[2] School of Hydraulic Engineering, Faculty of Infrastructure Engineering,
Dalian University of Technology, Dalian, 116024, China

Abstract

Recent studies on the moment whirl due to leakage flow in the back shroud clearance of hydro-turbine runners or centrifugal pump impellers are summarized. First, destabilizing effect of leakage flow is discussed for lateral vibrations using simplified models. Then it is extended to the case of whirling motion of an overhung rotor and the criterion for the instability is obtained. The fluid moment caused by a leakage clearance flow between a rotating disk and a stationary casing was obtained by model tests under whirling and precession motion of the disk. It is shown that the whirl moment always destabilizes the whirl motion of the overhung rotor while the precession moment destabilizes the precession only when the precession speed is less than half the rotor speed. Then vibration analyses considering both whirl and precession are made by using the hydrodynamic moments determined by the model tests. For larger overhung rotors, the whirl moment is more important and cause whirl instability at all rotor speed. On the other hand, for smaller overhung rotors, the precession moment is more important and cancels the destabilizing effect of the whirl moment.

Keywords: Rotordynamic Instability, Fluid Force Moment, Whirling Motion, Precession Motion, Leakage Flow

1. Introduction

Severe flexural vibration of the rotor shaft of a Francis turbine generator shown in Fig.1 was experienced in its test operation and reported by Tomita and Kawamura [1]. The mechanism of vibration is explained as follows [2]. Figure 2 shows the leakage flow model. As long as the runner remains in the center of the casing, the leak flow is uniform around the runner. Once the runner deviates from the center of the casing by y_1, the uniformity will be broken and the resulting change of the leak flow, represented by q in Fig.2 will occur in the back chamber. When the runner vibrates, the variational flow must change its direction accordingly, thus causing the variation of the pressure in the chamber. As the first step of understanding, the rotor is modeled by a plate with an entrance orifice and the leakage flow is modeled by a one-dimensional flow as shown in Fig.3. We assume that the leakage flow rate q is proportional to the leakage flow velocity U in the entrance orifice and the width B and the height y, i.e., $q = BU \cdot y$. The pressure distribution caused by the acceleration of the leakage flow rate is given by $p(x) = \rho \cdot (L - x) / (BH) \cdot \dot{q}$. Then the equation of motion of the plate can be expressed by

$$m\ddot{y} + c\dot{y} + ky = \int_0^L p(x)Bdx = \rho \frac{L^2}{2H}\dot{q} = \rho \frac{L^2}{2H} BU\dot{y} \tag{1}$$

This equation shows clearly that the pressure distribution caused by the acceleration of the leakage flow causes negative damping for the vibration of the plate.

Then, a lateral vibration model of an overhung rotor is proposed as shown in Fig.4. The upper end is rigidly supported and a bearing is placed at y_2. The lateral force on the rotor is represented by $P_h = A_f \dot{y}_1$ and the moment on the rotor by $M_h = A_m \dot{y}_1$. Here, the influence factors $\xi_{i,j}$ giving the lateral displacement at the node i due to the force at j, and $\eta_{i,j}$ giving the lateral displacement at the node i due to the moment at j are introduced. Then, the equation of motion can be expressed by

Received August 26 2010; accepted for publication September 6 2010: Review conducted by Prof. Tong-Seop Kim. (Paper number R10022K)
Corresponding author: Yoshinobu Tsujimoto, Professor, tujimoto@me.es.osaka-u.ac.jp

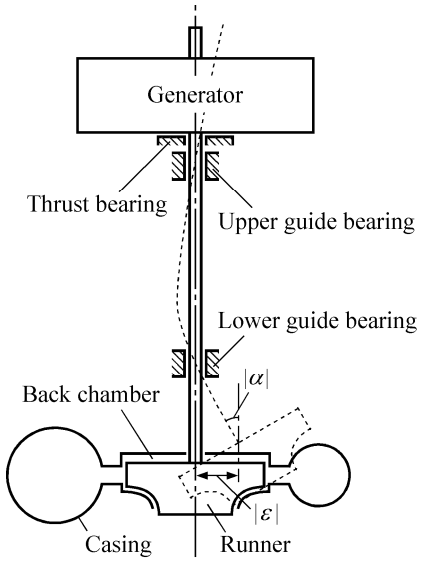

Fig. 1 Flexural vibration of a Francis turbine

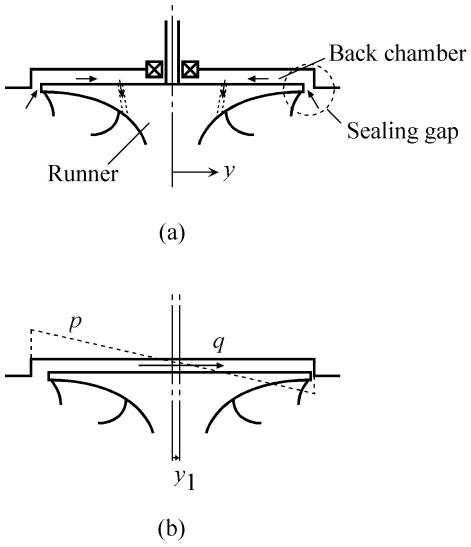

Fig. 2 Leakage flow model

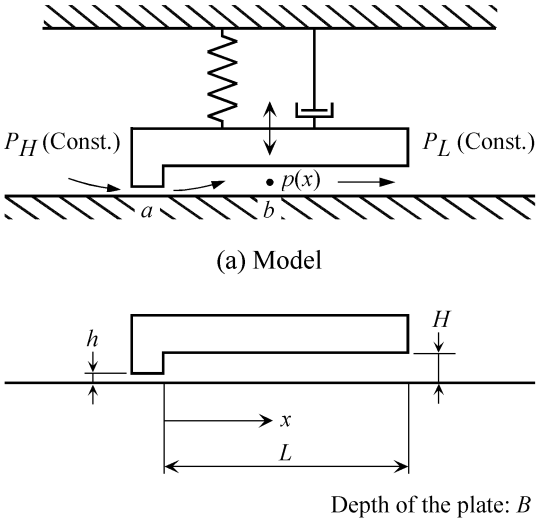

Fig. 3 One-dimensional flow model

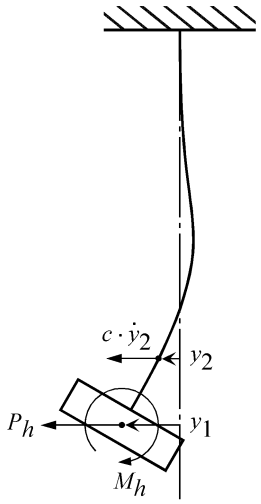

Fig. 4 Lateral vibration model

$$y_1 = \xi_{11}(-M\ddot{y}_1 + A_f \dot{y}_1) + \xi_{12}(-c\dot{y}_2) + \eta_{11}(A_m \dot{y}_1)$$
$$y_2 = \xi_{21}(-M\ddot{y}_1 + A_f \dot{y}_1) + \xi_{22}(-c\dot{y}_2) + \eta_{21}(A_m \dot{y}_1) \quad (2)$$

From these equations, it was shown that the lateral vibration grows when

$$c\xi_{21}{}^2 < (A_f + \frac{\eta_{11}}{\xi_{11}} A_m)\xi_{11}{}^2 \quad (3)$$

This result shows that fluid moment on the rotor can cause lateral vibration through structural coupling.

Thus, the possible mechanism of the vibration has been clearly shown by the simplified models. However, rotors generally exhibit whirling and precession motion and it is not clear under what conditions the self excited vibration occurs. Also the leakage flow in real geometry is not so simple as assumed in Fig.3. Simplified stability analysis is presented in section 2 to obtain the criterion of the whirl instability caused by whirl moments. In section 3, fluid moments due to whirl and precession are determined by model tests. Then, the vibration analysis under more general conditions with whirl and precession is described in section 4 using the fluid force moments determined in section 3.

2. Excitation of Whirl by Moment Through Structural Coupling

It is well known that rotor whirl can be caused by rotordynamic forces. However, it is not known under what conditions rotordynamic moment can cause whirl instabilities. We consider an overhung rotor rotating with an angular velocity ω and executing an whirling motion with an angular velocity Ω with a whirl radius $|\varepsilon|$ as shown in Fig.5(b) [3]. The fluid force F

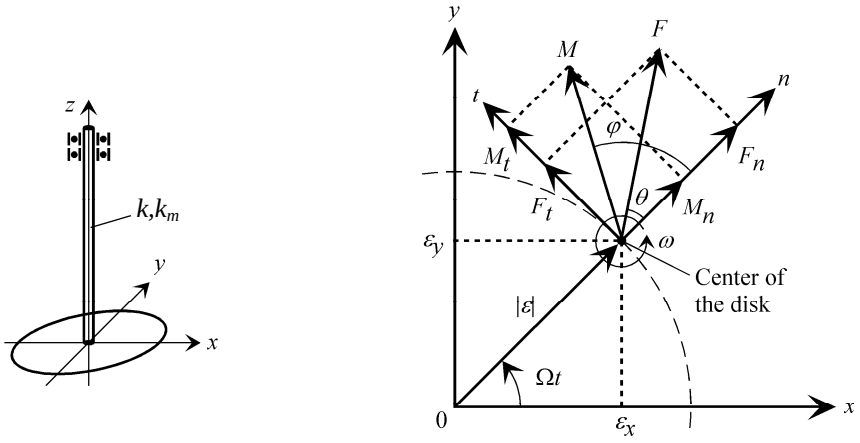

(a) Coordinate system

(b) Definition of the force and moment on complex plane, $z=x+iy$

Fig. 5 Force and moment acting on the rotor in whirling motion

and moment M are represented as follows

$$F = |\varepsilon| f e^{i(\Omega t+\theta)} = \varepsilon f e^{i\theta} \tag{4}$$

$$M = |\varepsilon| m e^{i(\Omega t+\varphi)} = \varepsilon m e^{i\varphi} \tag{5}$$

The displacement of the shaft ε caused by the force F^* and the moment M^* applied on the shaft by the rotor can be represented as follows, by using the stiffness coefficients k and k_m of the shaft.

$$\varepsilon = F^* / k + iM^* / k_m \tag{6}$$

If we consider the inertia $-m_a\ddot{\varepsilon}$ and the damping force on the rotor $-c\dot{\varepsilon}$, the momentum equation of the rotor for the lateral vibration can be given by

$$F^* = F - m_a\ddot{\varepsilon} - c\dot{\varepsilon} \tag{7}$$

If we assume that the angular displacement of the rotor is so small that the inertia moment can be neglected, we can write

$$M^* = M \tag{8}$$

If we put equations (6) and (8) into (7), we obtain

$$m_a\ddot{\varepsilon} + c\dot{\varepsilon} + k\varepsilon = F + i\frac{k}{k_m}M \equiv \varepsilon\left[\left(f_n - \frac{k}{k_m}m_t\right) + i\left(f_t + \frac{k}{k_m}m_n\right)\right] \equiv \varepsilon f_e e^{i\theta^*} \tag{9}$$

where,

$$f_n = f\cos\theta,\ f_t = f\sin\theta,\ m_n = m\cos\varphi,\ m_t = m\sin\varphi,$$

$$f_e = |f_{en} + if_{et}|,\quad f_{en} = f_n - (k/k_m)m_t,\ f_{et} = f_t + (k/k_m)m_n$$

Then, Eq.(9) can be rewritten as

$$m_a\ddot{\varepsilon} + c\dot{\varepsilon} + (k - f_e e^{i\theta^*})\varepsilon = 0 \tag{10}$$

If we put $\varepsilon = e^{\lambda t}$ in Eq.(10), and assume that c and f_e are sufficiently small, we obtain

$$\lambda = -\frac{c}{2m_a} \mp \frac{k_I}{2\sqrt{m_a k_R}} \pm i\sqrt{\frac{k_R}{m_a}} \tag{11}$$

where $k_R = k - f_e\cos\theta^*$ and $k_I = -f_e\sin\theta^*$. Equation (11) shows that the whirl frequency Ω is given by

$$\Omega = \Omega_R = \pm\sqrt{\frac{k_R}{m_a}} \tag{12}$$

The forward whirl with $\Omega_R = \sqrt{k_R / m_a}$ grows when

$$-\frac{c}{2m_a} - \frac{k_I}{2\sqrt{m_a k_R}} > 0$$

That is,

$$f_{et}\frac{1}{2m_a\Omega_R} > \frac{c}{2m_a} \quad \text{or} \quad |\varepsilon| f_{et} > c|\varepsilon|\Omega_R \tag{13}$$

This means that the whirl radius $|\varepsilon|$ grows when the equivalent tangential force $|\varepsilon| f_{et} = |\varepsilon|\{f_t + (k/k_m)m_n\}$ becomes larger than the damping force $c|\varepsilon|\Omega_R$. Equation (11) also shows that the backward whirl with $\Omega_R = -\sqrt{k_R / m_a}$ occurs when $|\varepsilon| f_{et} < -c|\varepsilon|\Omega_R$. The contribution of the tangential force f_t was shown by Ohashi et al. [4]. Present result shows the whirl instability can occur when the normal moment m_n has the same sign as the whirl angular velocity Ω.

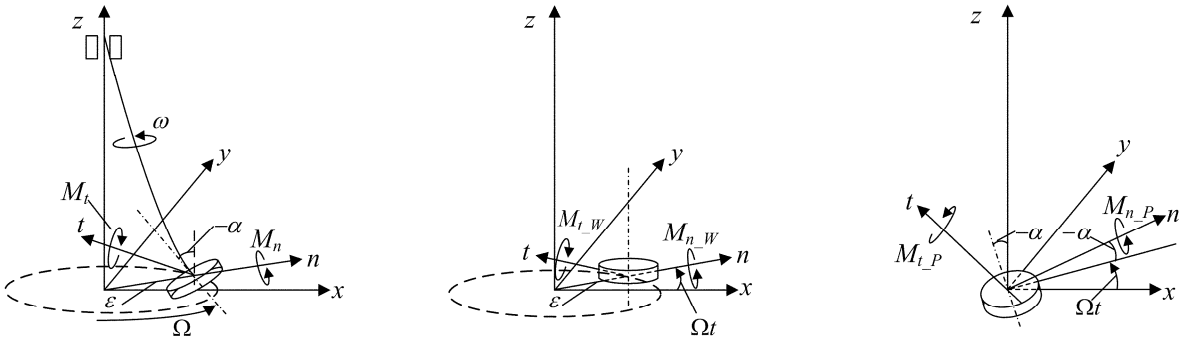

(a)Whirling and precession motions (b)Whirling motion (c)Precession motion

Fig. 6 Coordinate system

3. Rotordynamic Fluid Force Moment

As shown in Fig.6, the vibration of an over-hung rotor shown in (a) can be decomposed to the whirling motion shown in (b) and the precession motion shown in (c). As discussed in the last section, the hydrodynamic moment caused by the whirl motion is important in the moment whirl. However, the moment caused by the precession motion is also needed for general vibration analysis. So, both whirl moment and precession moment are measured. Figure 7 shows the experimental facility. The backshroud is modeled by a disk set close to the casing. Forced whirl/precession motion was given by a special bearing system supporting the shaft. The leakage flow was given by an external pump.

3.1 Whirling Moment

Figure 8 shows the whirl moment normalized by the reference moment $M_{0\omega} = \rho|\omega||\varepsilon| / C_2 \cdot (v_l \pi R_T^4)$ where C_2 =4mm is the axial clearance, v_l is the leakage flow velocity in the radial clearance C_1 =1mm and R_T =149.5mm is the radius of the disk [3]. U_j is the tangential velocity at the swirl generator and $U_T = R_T\omega$ is the disk tip speed. The moment was measured by the force balance attached to the shaft and also evaluated by the unsteady pressure distribution on the casing. The results agree reasonably. The moment was evaluated also numerically using a bulk flow model [5] in which the flow in the clearance is averaged over the clearance and the effect of wall stress is taken into account. Although significant difference is found, the tendency can be reproduced by the model. What is most important is that the sign on the normal

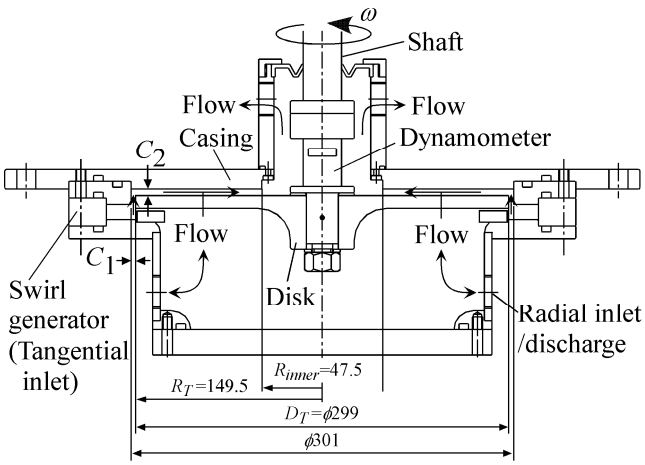

Fig. 7 Schematic of experimental facility

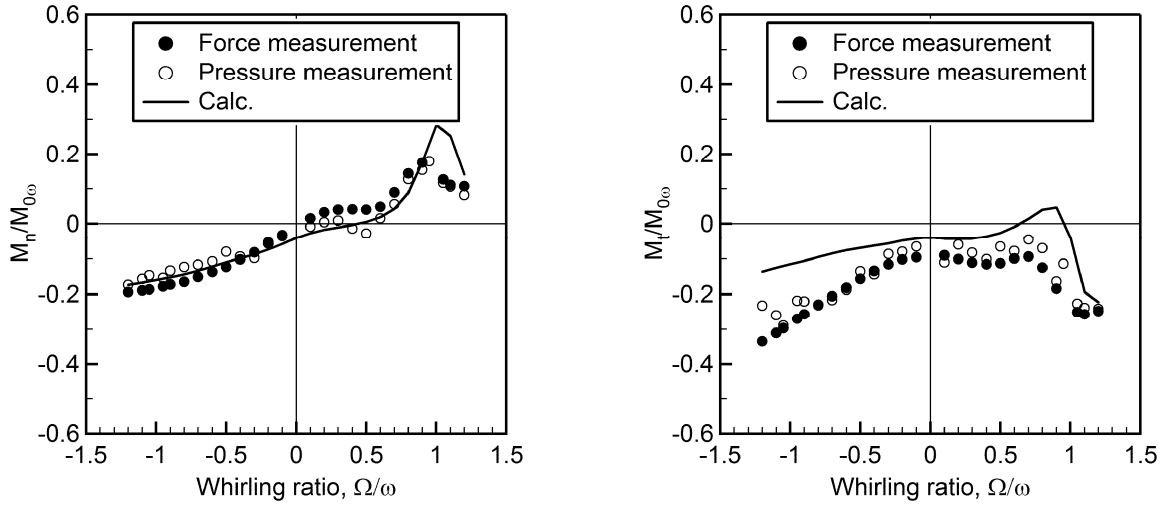

(a)Normal moment (b)Tangential moment

Fig. 8 Fluid force moments obtained by the force sensor, the steady pressure, and the computation in the case of whirling motion at v_l/U_T=0.170 and U_J/U_T =0 for C_2=4mm,

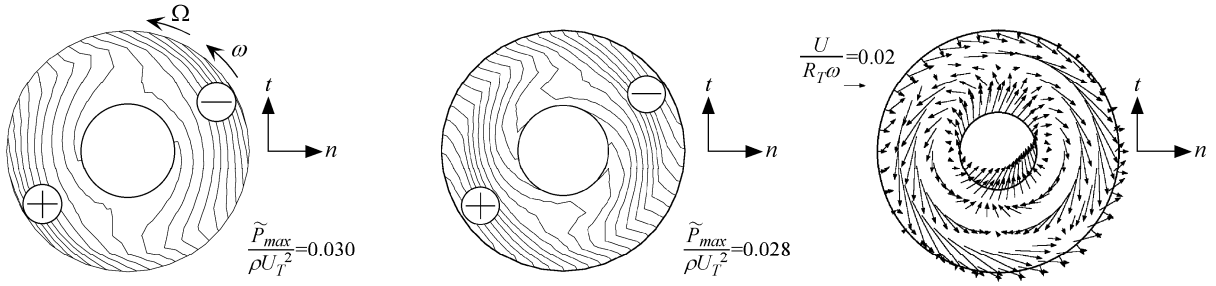

(a) Pressure (Exp.) (b) Pressure (Calc.) (c) Velocity (Calc.)

Fig. 9 Unsteady components of pressure and velocity in the clearance C_2=4mm in whirling motion at v_l/U_T=0.170 and U_J/U_T=0 for Ω/ω= 1.2

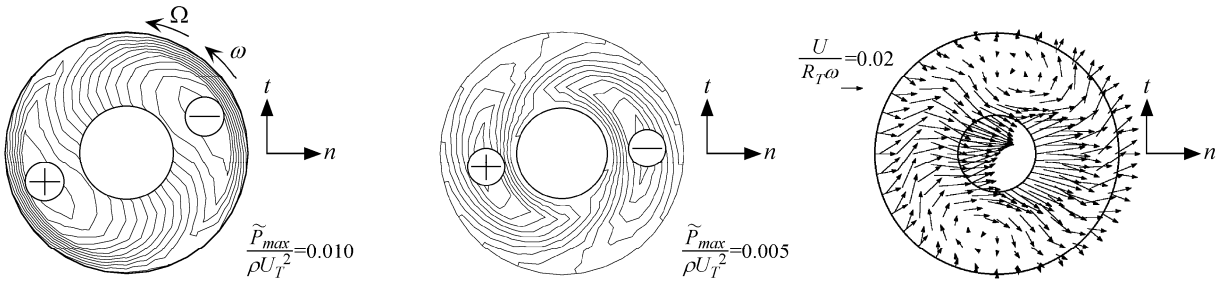

(a) Pressure (Exp.) (b) Pressure (Calc.) (c) Velocity (Calc.)

Fig. 10 The same as Fig.9, for Ω/ω= 0.3

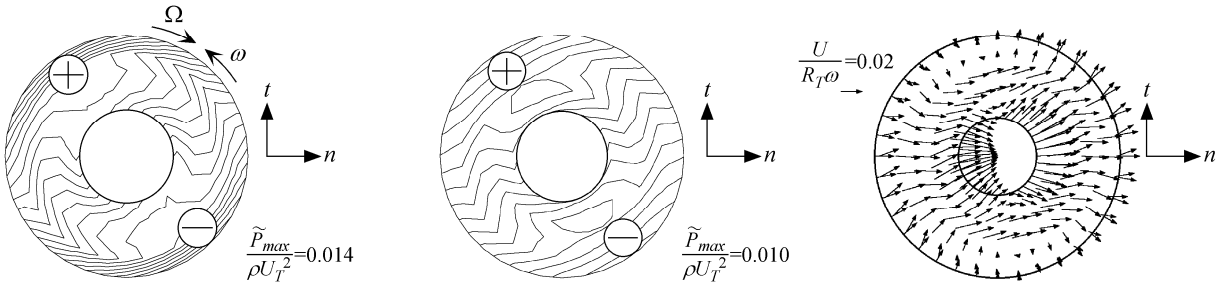

(a) Pressure (Exp.) (b) Pressure (Calc.) (c) Velocity (Calc.)

Fig. 11 The same as Fig.9, for Ω/ω= -0.3

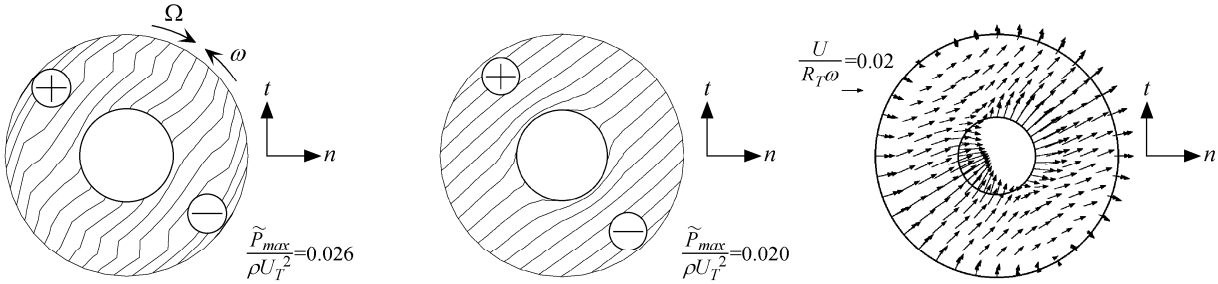

(a) Pressure (Exp.) (b) Pressure (Calc.) (c) Velocity (Calc.)

Fig. 12 The same as Fig.9, for Ω/ω= -1.2

moment M_n is the same as that of the whirl speed ratio Ω/ω, at almost all Ω/ω. This means that the whirl moment is always destabilizing the whirling motion.

Figures 9-12 show the pressure and disturbance velocity distributions, viewed from upper side in Fig.7. The normal direction (*n*) is displayed to the right, and the radial clearance is the smallest in this direction. At the periphery of the disk, the disturbance velocity vector is outward on the right hand side where the seal clearance is smaller. The experimental pressure distribution shown in (a) is qualitatively similar to the numerical results in (b). Generally, the pressure minimum occurs on the right hand side, where the seal clearance is smaller, caused by the larger resistance there. However, the location of the pressure minimum is tilted upward at $\Omega/\omega > 0$ and downward at $\Omega/\omega < 0$. At $\Omega/\omega > 0$, the leakage flow is decreasing on the upper half and decreasing on the lower half at $\Omega/\omega < 0$. Then the pressure is decreased in the upper half at $\Omega/\omega > 0$ and in the lower half at $\Omega/\omega < 0$, due to

the inertia effects. Since the normal moment is caused by the asymmetry of the pressure distribution across the horizontal axis, we can conclude the destabilizing normal moment is caused by the inertia effects of the leakage flow. This agrees with the result of simplified one dimensional model shown in Fig.3.

3.2 Precession Moment

Normal and tangential moment under precession motion is defined in Fig.13 and shown in Fig.14 [6]. The reference fluid moment is defined by $M_0 = \rho R_T^5 \omega^2 (R_T |\alpha| / C_2)$ where $\alpha = 0.48\,\text{deg} = 8.37\times10^{-3}\,\text{rad}$ is the tilt angle of the precession motion as shown in Fig.13. The axial clearance is the smallest in the normal direction but the radial seal clearance is the same at all circumferential locations. The stability analysis of the precession motion similar to the one described in section 2 for the whirling motion

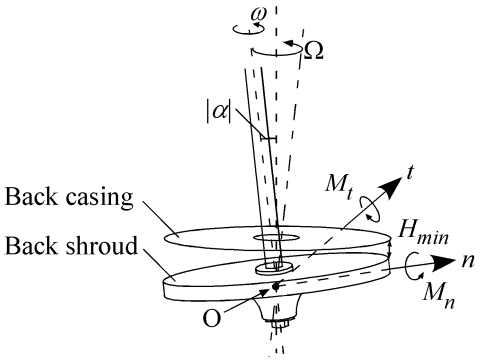

Fig. 13 Definition of the rotordynamic fluid force moment in precession motion

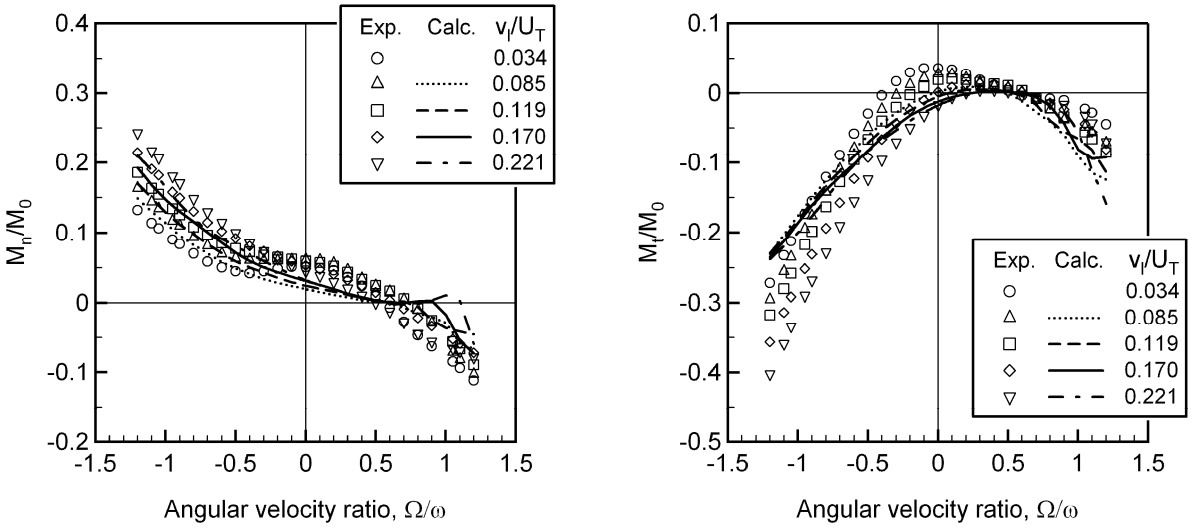

(a) Normal moment (b) Tangential moment

Fig. 14 Fluid force moment at various flow rates in precession motion for C_2=4mm and U_J/U_T=0

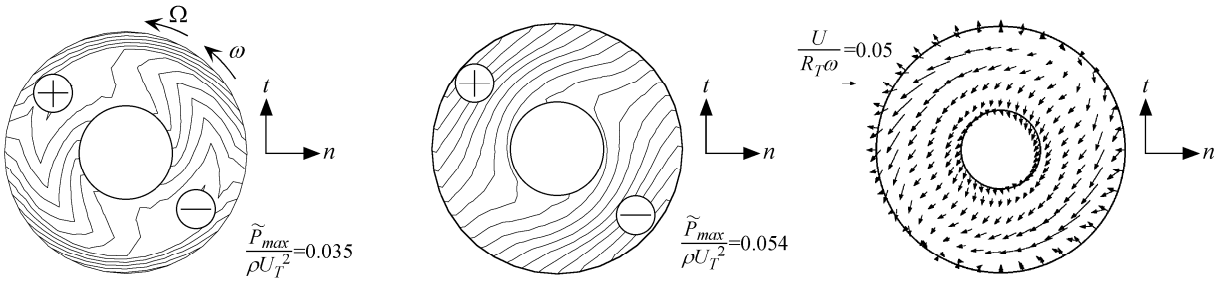

(a) Pressure (Exp.) (b) Pressure (Calc.) (c) Velocity (Calc.)

Fig. 15 Unsteady components of pressure and velocity in the clearance C_2=4mm in precession motion at v_l/U_T=0.170 and U_J/U_T=0 for Ω/ω=1.2

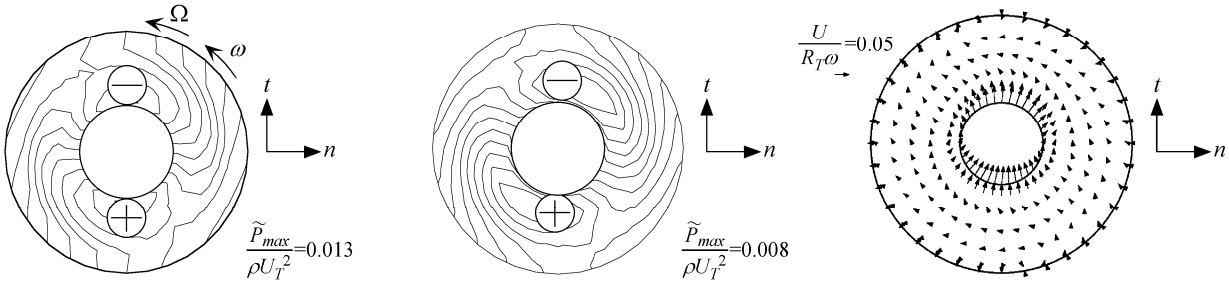

(a) Pressure (Exp.) (b) Pressure (Calc.) (c) Velocity (Calc.)

Fig. 16 The same as Fig. 15, for Ω/ω=0.3

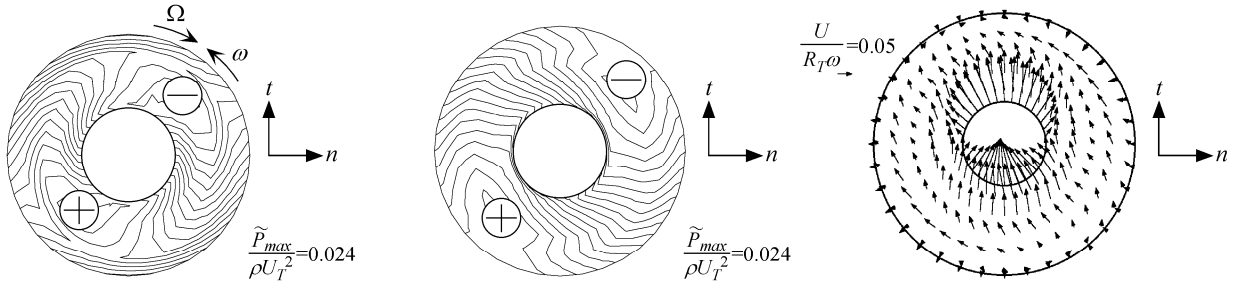

(a) Pressure (Exp.) (b) Pressure (Calc.) (c) Velocity (Calc.)

Fig. 17 The same as Fig. 15, for Ω/ω=-0.3

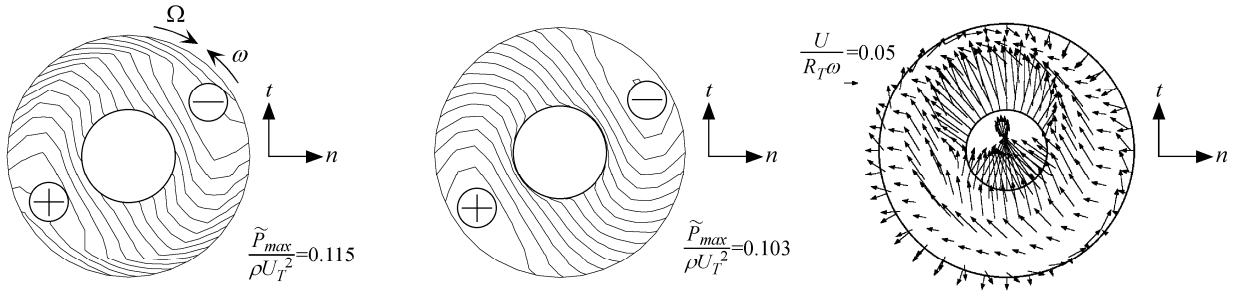

(a) Pressure (Exp.) (b) Pressure (Calc.) (c) Velocity (Calc.)

Fig. 18 The same as Fig. 15, for Ω/ω=-1.2

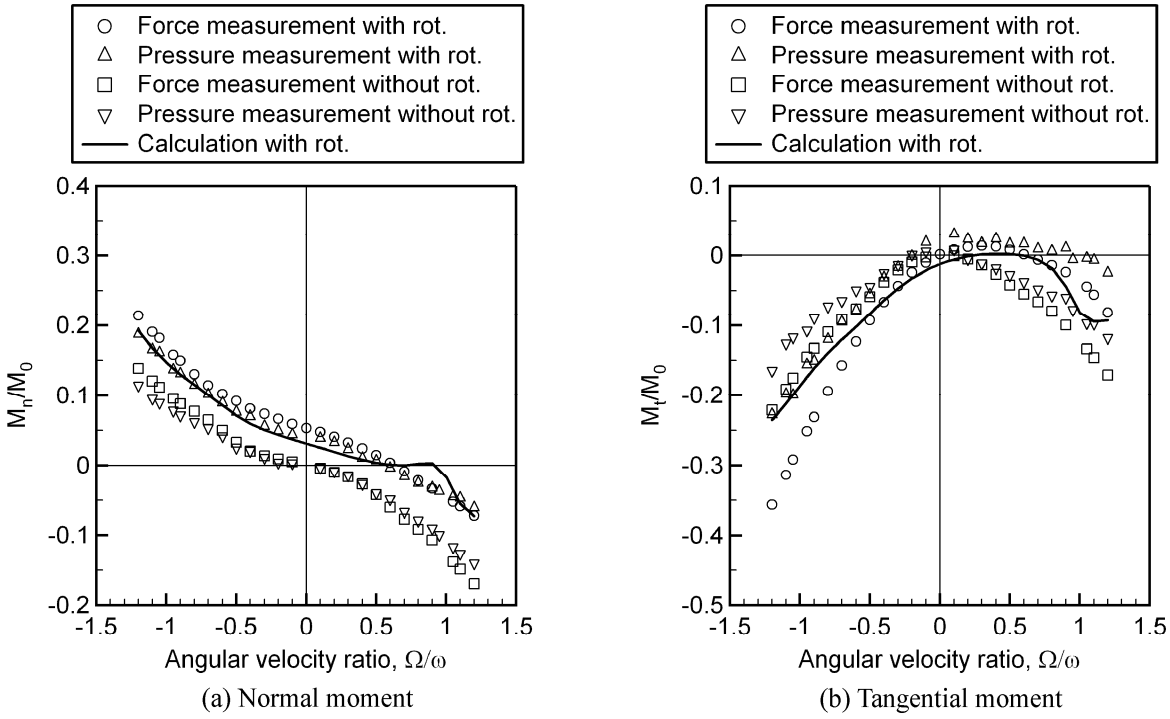

(a) Normal moment (b) Tangential moment

Fig. 19 Comparison of fluid force moments obtained by the force sensor, the unsteady pressure, and the computation between the conditions of precession with and without rotation at v_l/U_T=0.170 and U_J/U_T=0 for C_2=4mm

shows that the precession is promoted when the normal moment has the same sign as the precession speed ratio Ω/ω. Figure 14(a) shows that the precession is destabilized in the region $0<\Omega/\omega\le 0.5$.

Figures 15-18 show the pressure and the disturbance velocity of the clearance flow. In these figures, the axial clearance is the smallest on the right and the directions of disk rotation and precession are shown in the figure. Higher pressure region is in the upper part for $\Omega/\omega>0.5$ and in the lower part for $\Omega/\omega<0.5$. This is caused by the relative circumferential flow with the angular velocity $\omega/2-\Omega$ passing through the circumferential location with smaller axial clearance at *n*-direction. The radial velocity disturbance near the outer radius is negative on the right hand side where the axial clearance is smaller, at all Ω/ω. This

is because the leakage velocity is increased in the region with smaller axial clearance since the leakage flow rate is kept nearly constant by larger resistance of smaller radial clearance C_1=1mm, which is kept nearly constant under precession. Near the inner radius, upward velocity is observed when $\Omega/\omega < 0.5$ and the magnitude becomes larger when $|1/2-\Omega/\omega|$ becomes larger. On the other hand, downward velocity is observed at $\Omega/\omega = 1.2 > 0.5$. The inward velocity at the inner radius occurs when the relative circumferential flow with the angular velocity $\omega/2-\Omega$ passes through the region where the clearance decreases, so that the continuity equation is satisfied.

As discussed above, the tangential flow caused by the disk rotation plays an important role in producing the precession moment. In order to show the effects more clearly, tests were carried out without the disc rotation. Figure 19 compares the moment with and without the disk rotation. Comparison of the results from force measurement and the pressure measurement, as well as from numerical calculation is shown. Without the rotation, the tangential moment is decreased by a constant amount over all Ω/ω and the destabilizing region in $0 < \Omega/\omega \le 0.5$ disappears. This clearly shows the importance of the tangential flow caused by the disk friction. Without disk rotation, both normal and tangential components are nearly symmetrical with respect to $\Omega/\omega = 0$.

4. Vibration Analysis Including both Whirl and Precession Motion

In the simplified stability analysis in section 2, the effects of precession are neglected to highlight the destabilization of whirling motion by the whirl moment. A more complete analysis using a lumped parameter model is carried out in this section taking account of both whirl and precession motion and associated fluid moment evaluated in section 3. We consider an overhung shaft simply as an stiffness element to the linear displacement $\varepsilon = \tilde{\varepsilon} e^{j\Omega t}$ and the angular displacement $A = -j\tilde{\alpha} e^{j\Omega t}$. Then, the momentum equations can be represented by

$$M_d \ddot{\varepsilon} + K_{11}\varepsilon - jK_{12}A = F_f \tag{14}$$

$$I_d \ddot{A} + K_{22}A + jK_{21}\varepsilon = M_f + M_G \tag{15}$$

where, F_f and M_f are fluid force and moment, $M_G = j\omega I_p \dot{A}$ is the gyroscopic moment [7]. M_d and I_d are the mass and the moment of inertia of the disk, respectively. K_{ij} are stiffness coefficients for lateral and angular displacements. The values of K_{ij} are determined by assuming an overhung rotor. The fluid force and the gyroscopic moment are neglected here for simplicity. The fluid force moment components determined in section 3 are fitted with parabolic curves in terms of the speed ratio Ω/ω.

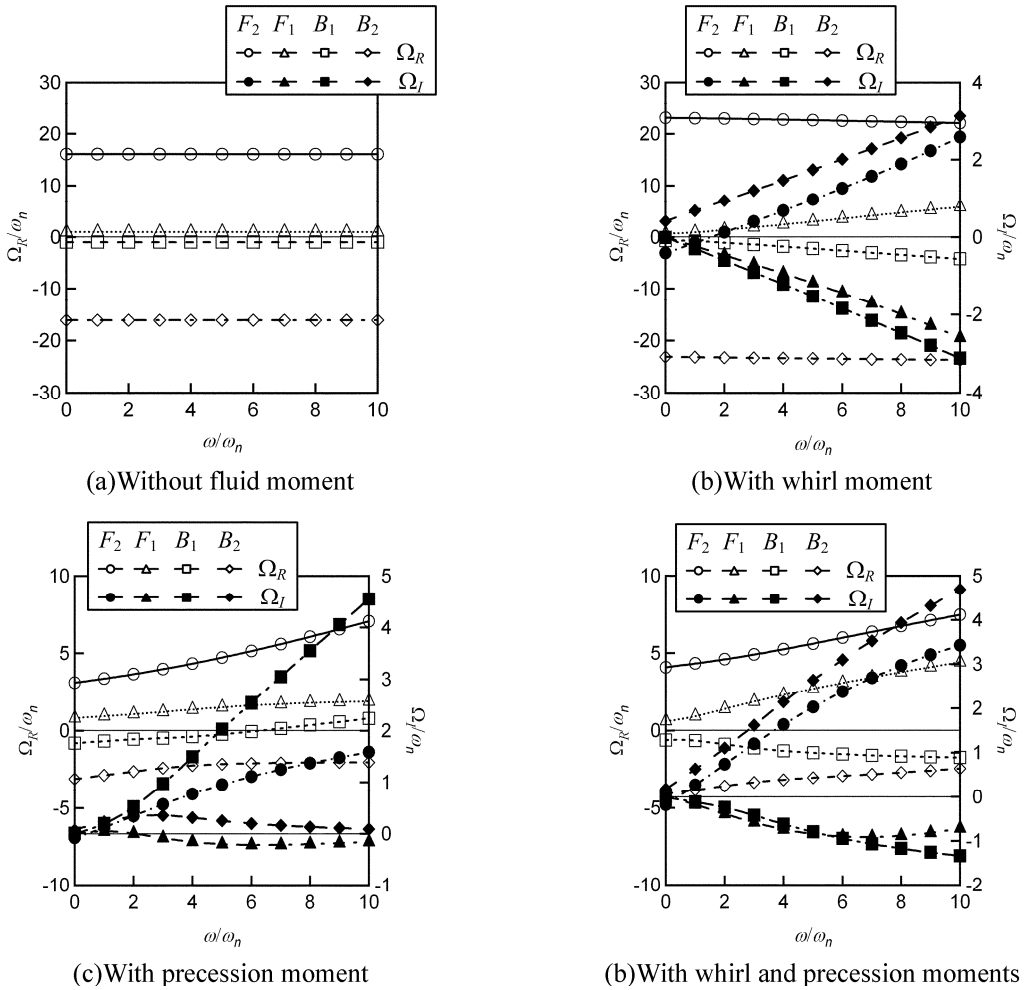

(a)Without fluid moment (b)With whirl moment

(c)With precession moment (b)With whirl and precession moments

Fig. 20 The effects of fluid force moments on the complex frequency of the rotor-shaft system at v_l/U_T=0.170, U_J/U_T=0 for L/D_T=3.344, C_2=4mm,

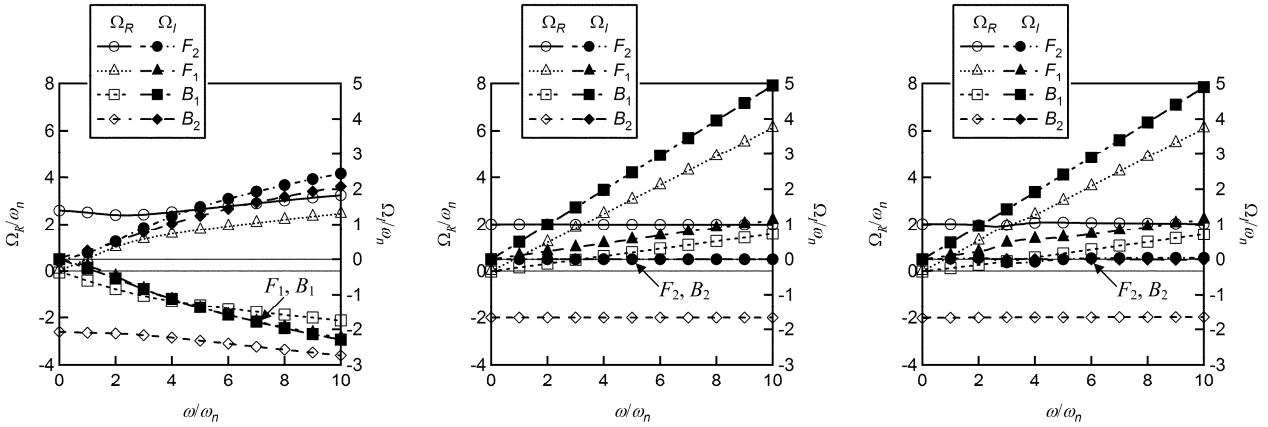

(a)With whirl moment (b)With precession moment (c)With whirl and precession moments

Fig. 21 The complex frequency in the case of shaft length L/D_T=0.033

Then, the moment can be represented by components proportional to ε, $\dot{\varepsilon}$, $\ddot{\varepsilon}$ and A, $\dot{A}$, $\ddot{A}$. By using this expression, Eqs.(14) and (15) can be represented by a system of homogeneous linear equations in terms of $\tilde{\varepsilon}$ and $\tilde{\alpha}$. By putting the determinant of the coefficient matrix to be zero, a fourth order characteristic equation in terms of the complex frequency $\Omega = \Omega_R + j\Omega_I$ is obtained. Numerical calculations were made for the experimental facility assuming different overhung length L.

Figure 20 shows the complex frequencies $\Omega = \Omega_R + j\Omega_I$ for the case of overhung length to disk diameter ratio $L/D_T = 3.344$. F_1 and F_2 shows the first and second order forward modes with $\Omega_R > 0$, B_1 and B_2 the first and second order backward modes with $\Omega_R < 0$. The imaginary part Ω_I shows the damping rate and the amplitude grows when $\Omega_I < 0$. The disk rotational speed ω and the complex frequency components Ω_R and Ω_I are normalized by the natural frequency $\omega_n = (1/2)\sqrt{K_{11}/M_d}$ of lateral vibration. If we consider only the whirl moment, as shown in Fig.20(b), the first order forward and backward modes (F_1 and B_1) are amplified at all rotational speed. This agrees with the result shown in Fig.8 that the whirl moment is always destabilizing. If we consider only the precession moment, as shown in Fig.20(c), F_1 becomes destabilizing in the region with $\omega/\omega_n > 2$. This region corresponds to $\Omega_R/\omega < 0.5$ where the normal precession moment becomes positive in Fig.14. The results with both whirl and precession moments shown in Fig.20(d) is similar to the case with only whirl moment shown in Fig.20(b). This shows that the whirl moment is more important than the precession moment for the case with $L/D_T = 3.344$ and that the simplified stability criteria obtained in section 3 can be applied.

Figure 21 shows the results for the case of extremely small overhung rotor with $L/D_T = 0.033$. With only the whirl moment, shown in Fig.21(a), F_1 and B_1 are amplified at all rotational speed. On the other hand, with only the precession moment, shown in Fig.21(b), all modes are damped. This is because the value of $\Omega_R/\omega \approx 0.62$ for F_1 is larger than 0.5. With both whirl and precession moments, shown in Fig.21(c), the results are similar to the results with only precession moment. This shows that the precession moment is more important than the whirl moment for the case with small overhung rotors.

As described above, the criteria obtained by the simplified stability analysis in section 3 can be applied to the first order modes. However, detailed examination on the second order components shows that there are certain cases when the simplified criteria cannot be applied. This was found to be caused by larger fluid moment. If the fluid force moment was decreased to 1/1000 of the experimental values, it was found that the results of section 3 can be applied reasonably for all cases.

5. Conclusions

It was shown by a simplified model that the whirl moment on an overhung rotor destabilizes the whirl motion through structural coupling if the normal component of the moment has the same sign as the whirl speed ratio. From the measurement of whirl moment, it was found that the whirl moment is destabilizing the whirl motion at all whirl speed ratio, caused by the inertia on the leakage flow. Thus the leakage flow is more important in the destabilizing effects of whirl moment. The precession moment is destabilizing the precession in the region of $0 < \Omega/\omega \le 0.5$ caused by the interaction of tangential flow due to disk rotation with the variation of the axial clearance. So the tangential flow is important for the destabilization of the precession motion. From the vibration analysis of overhung rotors considering both whirl and precession, it was found that the whirl moment is more important for the rotors with larger overhung and the whirl moment destabilizes the whirl motion at all rotor speed. This shows that sufficient damping is always needed for the rotors with similar seal geometry as studied here. For smaller overhung rotors, the precession moment is more important than the whirl moment and the destabilizing effect of whirl moment is damped by the stabilizing effect of precession moment. The above results can be directly applied only to the case of leakage flow between rotating disc and stationary casing. However, there can be other cases when the fluid force moment destabilizes the whirl motion through structural coupling.

6. Acknowledgements

The lead author would like to express his special thanks to Prof. Hideo Ohashi. The authors learned about the present interesting problem from his book [2]. The stability analysis in section 3 is based on his pioneering work [4]. The experimental facility was developed and built by him and was given to the lead author in 1992 on his retirement from University of Tokyo. So, the present work totally depends on him and shows that a carefully designed facility is useful over decades.

References

[1] Tomita, H. and Kawamura, M., 1965, ‘‘Self-Excited Vibration in Francis Turbines,’’ Toshiba Review, Vol. 20, No. 8, pp. 787-791. (in Japanese)
[2] Ohashi, H., 1991, ‘‘Vibration and Oscillation of Hydraulic Machinery (International Hydraulic machinery Series),’’ Avebury Technical, Aldershot.
[3] Song, B., Horiguchi, H., Ma, Z., and Tsujimoto, Y., 2010, “Rotordynamic Moment on the Backshroud of a Francis Turbine Runner Under Whirling Motion,” ASME Journal of Fluids Engineering, Vol. 132, pp. 071102_1-071102_9.
[4] Shoji, H. and Ohashi, H., 1981, ‘‘Hydrodynamic Forces on Whirling Centrifugal Impeller,’’ (in Japanese), Trans. JSME, Series B, Vol. 47, No. 419, pp. 1187-1196.
[5] Childs, D. W., 1989, ‘‘Fluid-Structure Interaction Forces at Pump-Impeller-Shroud Surfaces for Rotordynamic Calculations,’’ ASME, J. Vibration, Acoustics, Stress, and Reliability in Design, Vol. 111, pp. 216-225.
[6] Song, B., Horiguchi, H, Nishiyama, Y., Hata, S., Ma, Z., and Tsujimoto, Y., 2010, “Fluid Force Moment on the Backshroud of a Francis Turbine Runner in Precession Motion,” ASME Journal of Fluids Engineering, Vol. 132, pp. 051108_1-051108_8.
[7] Song, B., Horiguchi, H., Ma, Z., and Tsujimoto, Y., 2010, “Rotordynamic Instabilities Caused by the Fluid Force Moments on the Backshroud of a Francis Turbine Runner,” International Journal of Fluid Machinery and Systems, Vol. 3, No. 1, pp. 67-79.

Yoshinobu Tsujimoto B.E.(1971), M.E.(1973), Dr.Eng(1977) from Osaka University, Research Associate of Engineering Science , Osaka University (1977), Associate Professor of Engineering Science, Osaka University (1986), Professor of Engineering Science, Osaka University (1989-).

Zhenyue Ma B.E.(1982), M.E.(1985), Dr.Eng(1988) from Dalian University of Technology, Lecturer of the Department of Civil Engineering of Dalian University of Technology(1985). Associate Professor of Department of Civil Engineering in Dalian University of Technology (1990). Professor of School of Civil and Hydraulic Engineering in Dalian University of Technology (1995-).

Bingwei Song is a joint PhD student of Dalian University of Technology and Osaka University. He received his Bachelor Degree in the Department of Civil Engineering from North China Institute of Water Conservancy and Hydro-Electric Power, Zhengzhou, China, in 2005. Then he passed the qualification exam and became a Master-Doctor Combined Program Graduate Student. And he will receive his Doctoral Degree in the School of Hydraulic Engineering from Dalian University of Technology, Dalian, China, in 2010.

Hironori Horiguchi Bachelor (1995), Master (1997), and Ph.D (1999) in Engineering from Osaka University, Research Associate in the Faculty of Engineering, Tokushima University, Tokushima, Japan (1999), Associate Professor in the Graduate School of Engineering Science, Osaka University, Osaka, Japan (2003-).